Modulation of activity by Arg407: structure of a fungal α-1,2-mannosidase in complex with a substrate analogue

Yuri D. Lobsanov,[a] Takashi Yoshida,[b] Tom Desmet,[c] Wim Nerinckx,[c] Patrick Yip,[a] Marc Claeyssens,[c] Annette Herscovics[d] and P. Lynne Howell[a,e]*

[a]Program in Molecular Structure and Function, Research Institute, The Hospital for Sick Children, 555 University Avenue, Toronto, Ontario M5G 1X8, Canada, [b]Department of Biochemistry and Biotechnology, Hirosaki University, Aomori 036-8560, Japan, [c]Laboratory for Biochemistry, Department of Biochemistry, Physiology and Microbiology, Ghent University, K. L. Ledeganckstraat 35, B-9000 Ghent, Belgium, [d]The McGill Cancer Centre, McGill University, 3655 Promenade Sir-William-Osler, Montréal, Québec H3G 1Y6, Canada, and [e]Department of Biochemistry, University of Toronto, Toronto, Ontario M5S 1A8, Canada

Correspondence e-mail: howell@sickkids.ca

Class I α-mannosidases (glycoside hydrolase family GH47) play key roles in the maturation of N-glycans and the ER-associated degradation of unfolded glycoproteins. The 1.95 Å resolution structure of a fungal α-1,2-mannosidase in complex with the substrate analogue methyl-α-D-lyxopyranosyl-(1′,2)-α-D-mannopyranoside (LM) shows the intact disaccharide spanning the −1/+1 subsites, with the D-lyxoside ring in the −1 subsite in the $^1C_4$ chair conformation, and provides insight into the mechanism of catalysis. The absence of the C5′ hydroxymethyl group on the D-lyxoside moiety results in the side chain of Arg407 adopting two alternative conformations: the minor one interacting with Asp375 and the major one interacting with both the D-lyxoside and the catalytic base Glu409, thus disrupting its function. Chemical modification of Asp375 has previously been shown to inactivate the enzyme. Taken together, the data suggest that Arg407, which belongs to the conserved sequence motif RPExxE, may act to modulate the activity of the enzyme. The proposed mechanism for modulating the activity is potentially a general mechanism for this superfamily.

1. Introduction

Protein glycosylation is a major post-translational modification that modulates the structure and function of secretory and membrane proteins and participates in a wide variety of intracellular and extracellular biological processes (for reviews, see Varki, 1993; Helenius & Aebi, 2004; Trombetta & Parodi, 2003; Lowe & Marth, 2003; Haltiwanger & Lowe, 2004; Spiro, 2004). The carbohydrates influence protein folding and stability and participate in endoplasmic reticulum (ER) quality control, ensuring that cells maintain only properly folded glycoproteins and that abnormal glycoproteins are degraded in a process known as ERAD (Helenius & Aebi, 2004).

Class I α-1,2-mannosidases are inverting enzymes that belong to family GH47 of the glycoside hydrolase classification (http://www.cazy.org; Henrissat & Bairoch, 1996). Members of this protein family can be divided into three distinct subgroups. Subgroup 1 and 2 enzymes are required for the maturation of N-glycans from high-mannose to complex or hybrid structures (for reviews, see Herscovics, 1999, 2001). Subgroup 1 includes the yeast and mammalian ER α-1,2-mannosidases that preferentially form $Man_8GlcNAc_2$ isomer B (lacking a mannose on the middle branch of the oligosaccharide) from $Man_9GlcNAc_2$ (Camirand et al., 1991; Gonzalez et al., 1999; Tremblay & Herscovics, 1999; Fig. 1a). Subgroup 2 includes three mammalian Golgi α-1,2-mannosidases, as well as the fungal enzymes that form $Man_8GlcNAc_2$

isomers A and/or C from $Man_9GlcNAc_2$ (Lal *et al.*, 1998; Tremblay & Herscovics, 2000), while subgroup 3 proteins such as the mammalian EDEMs 1–3 and yeast Htm1p/Mnl1p take part in ERAD of misfolded glycoproteins (Olivari & Molinari, 2007; Hosokawa *et al.*, 2001; Jakob *et al.*, 2001; Nakatsukasa *et al.*, 2001; Mast *et al.*, 2005; Olivari *et al.*, 2005). Although EDEM1 and EDEM3 have recently been shown to have hydrolytic activity *in vivo* (Hirao *et al.*, 2006; Olivari *et al.*, 2006), to date no activity has been demonstrated for subgroup 3 proteins *in vitro* (Hosokawa *et al.*, 2001; Mast *et al.*, 2005).

The structures of several class I α-1,2-mannosidases have been determined, beginning with the prototypic yeast ER enzyme (Vallée, Lipari *et al.*, 2000). They all consist of an $(\alpha\alpha)_7$ barrel in which the catalytic site is located deep within the barrel above a β-hairpin that plugs the barrel at one end, forming a cavity ~ 15 Å deep. Detailed structural comparisons show that all the conserved acidic amino-acid residues in the active site as well as the essential calcium ion are superimposable (Vallée, Karaveg *et al.*, 2000; Lobsanov *et al.*, 2002; Tempel *et al.*, 2004), indicating that subgroup 1 and subgroup 2 enzymes have the same catalytic mechanism. Their differing specificity depends on nonconserved amino acids in the oligosaccharide-binding site that modulate the accessibility of different branches of the oligosaccharide substrate to the catalytic site (Lobsanov *et al.*, 2002; Tempel *et al.*, 2004). The structure of a representative member of subgroup 3 has not yet been determined.

We have previously determined the structures of subgroup 1 and 2 α-1,2-mannosidases complexed with kifunensine (KIF) or 1-deoxymanno-jirimycin (dMNJ) and showed that these inhibitors bind to the -1 subsite in a $^1C_4$ conformation (Lobsanov *et al.*, 2002; Vallée, Karaveg *et al.*, 2000). We proposed a catalytic mechanism for class I α-1,2-mannosidases involving acid–base catalysis with an unusual water-mediated proton donor. However, because the inhibitors used were monosaccharide mimics that only occupy one subsite, it was not possible to unambiguously identify the catalytic acid and base. To establish the details of the catalytic mechanism and the nature of the transition state of the substrate, the structure of a mannosidase complexed with a disaccharide-substrate

mimic spanning both -1 and $+1$ subsites was pursued. Here, we present the crystal structure of the subgroup 2 *Penicillium citrinum* α-1,2 mannosidase in complex with methyl-α-D-lyxopyranosyl-(1',2)-α-D-mannopyranoside (LM), an analogue of the minimal disaccharide substrate mannobiose (Fig. 1b). This complex shows the intact LM spanning the $-1/+1$ subsites with the D-lyxoside ring in the higher energy $^1C_4$ chair conformation and provides insight into the catalytic mechanism. An arginine residue, Arg407, is found in two alternative conformations, one of which directly interacts with
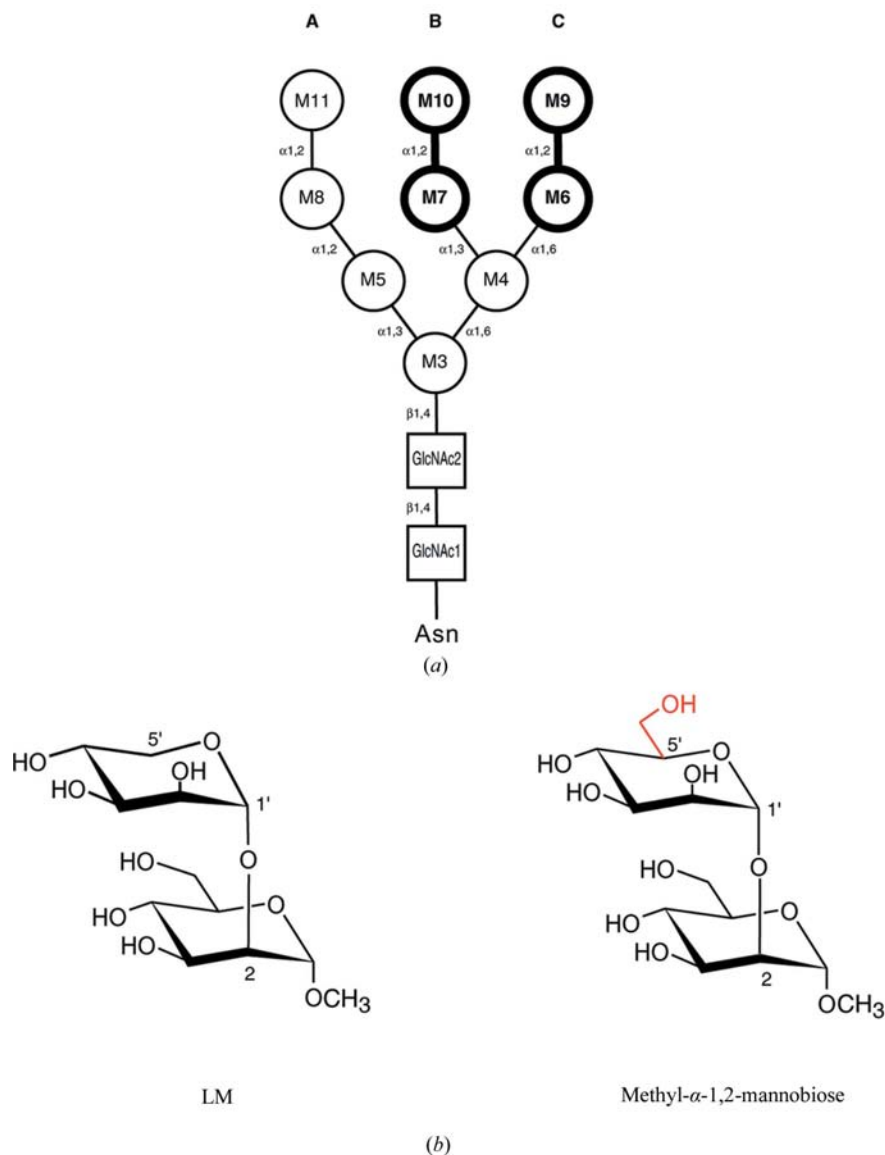

Figure 1
Schematic representation of (*a*) the high-mannose $Man_9GlcNAc_2$ N-glycan structure and (*b*) methyl-α-D-lyxopyranosyl-(1',2)-α-D-mannopyranoside (LM) and methyl-α-D-mannopyranosyl-(1',2)-α-D-mannopyranoside (methyl-α-1,2-mannobiose). The mannose residues in (*a*) are labelled M3–M11. Removal of a single mannose residue, M11, M10 or M9, results in the formation of $Man_8GlcNAc_2$ isomers A, B and C, respectively. The mannose moieties M7 and M6 observed in the $+1$ subsite in the yeast ER (Vallée, Karaveg *et al.*, 2000) and mouse Golgi mannosidase (Tempel *et al.*, 2004) structures, together with the corresponding α-1,2-linked mannose moieties, are highlighted in bold. The 5'-hydroxymethyl moiety of methyl-α-1,2-mannobiose in (*b*) is highlighted in red.

the catalytic base, thus disrupting its function. Chemical modification of the carboxylate residue that interacts with this arginine has previously been shown (Yoshida *et al.*, 1994) to directly affect activity. Taken together, the data suggest that this arginine may potentially modulate the activity of the enzyme.

2. Materials and methods

2.1. Sample preparation

Constructs for the expression of and methods for the purification of the soluble recombinant α-1,2-mannosidase from *P. citrinum* were as described in previous studies (Yoshida *et al.*, 1998; Lobsanov *et al.*, 2002). Briefly, the DNA of the *P. citrinum* α-1,2 mannosidase gene (*msdC*; Yoshida & Ichishima, 1995) lacking the signal sequence was cloned downstream of the *Aspergillus* amylase promoter (PamyB) and of the aspergillopepsin signal sequence. The resulting fungal expression vector pTAPM1 was transfected into *A. oryzae* strain MS2 (*argB$^-$*). An auxotrophic transformant was cultured in medium containing dextrin as an inducer. The medium was collected after 3 d culture at 303 K and the recombinant α-1,2-mannosidase, starting at amino acid 21, was purified from the medium by chromatography on CM-Toyo-pearl 650M after ammonium sulfate precipitation.

2.2. Crystallization and X-ray data collection

Crystals of both the native protein and the protein–inhibitor complex were grown at room temperature by the hanging-drop vapour-diffusion method. Equal volumes (1 µl) of native protein solution (18–20 mg ml^{-1} in 10 mM sodium acetate pH 5.0) and of well solution [15–18%(w/v) polyethylene glycol 6000, 100 mM HEPES pH 7.0] were mixed and suspended over 0.5 ml well solution. Isomorphous crystals of the protein were grown in the presence of the inhibitor under the same conditions as described above with the protein mixed and incubated with the inhibitor at a concentration of 5 mM for 30 min prior to crystallization setup. Prism-shaped crystals grew within a week to maximum dimensions of 0.3 × 0.2 × 0.2 mm. To obtain the protein–inhibitor complex with intact LM inhibitor (Fig. 1*b*), native protein crystals were soaked for a total of 10 min in a series of artificial mother-liquor solutions. The crystal was sequentially moved between four mother-liquor solutions that contained 26%(w/v) PEG 6000, 100 mM HEPES pH 7.0 and increasing concentrations of LM and glycerol. The initial solution contained 1 mM LM and 5%(v/v) glycerol and the final solution contained 9 mM LM and 20%(v/v) glycerol. A 10 min soak was chosen because longer soaks caused the crystals to shatter. Given the sequential addition of glycerol during the soaking process, no further cryoprotection was necessary prior to flash-freezing the crystals in a stream of nitrogen gas in preparation for data collection at 100 K. The cocrystals were cryoprotected by soaking for 1–2 min in the crystallization solution containing 20%(v/v) glycerol. Data were collected from the soaked crystal on beamline X-8C at the National Synchrotron Light

Table 1
Data-collection and refinement statistics.

Values in parentheses are for the highest resolution shell.

	Cocrystal	Soak
Space group	$P2_1$	$P2_1$
Unit-cell parameters (Å, °)	$a = 56.5,$	$a = 56.5,$
	$b = 111.0,$	$b = 111.0,$
	$c = 86.2,$	$c = 86.2,$
	$\beta = 99.2$	$\beta = 99.2$
Resolution (Å)	2.16 (2.24–2.16)	1.95 (2.02–1.95)
R_{merge}† (%)	8.3 (27.8)	8.9 (26.6)
No. of measured reflections	202119	392087
No. of unique reflections	52973	70492
Redundancy	3.8	5.6
Completeness (%)	98.0 (98.0)	95.9 (83.2)
Average $I/\sigma(I)$	10.6 (4.3)	37.1 (6.4)
$R_{\mathrm{cryst}}/R_{\mathrm{free}}$‡	20.6/27.4	21.0/26.0
No. of protein atoms	7450	7450
No. of waters	692	717
No. of ligand atoms§	44	70
No. of N-glycan atoms	234	234
R.m.s.d. bonds (Å)	0.009	0.012
R.m.s.d. angles (°)	1.45	1.49
Average B factor (Å^2)		
Protein	26.9	27.0
Ligand	32.9	18.8
Water	32.0	32.6
Ramachandran plot (%)		
Most favoured	85.5	85.8
Allowed	14.4	13.8
Cross-validated σ_A coordinate error (Å)	0.35	0.23

† $R_{\mathrm{merge}} = \sum_{hkl}\sum_i |I_i(hkl) - \overline{I(hkl)}|/\sum_{hkl}\sum_i I_i(hkl)$, where $I_i(hkl)$ is the measured intensity for each symmetry-related reflection and $\overline{I(hkl)}$ is the mean intensity for the unique reflection. The summation is over all unique reflections. ‡ $R_{\mathrm{cryst}} = \sum |F_o| - |F_c|/\sum F_o$ and $\sum |F_{os}| - |F_{cs}|/\sum F_{os}$, where 's' refers to a subset of data not used in the refinement, representing 7% of the total number of observations. § Ligand atoms refer to the Ca^{2+} ions and either LM and/or glycerol molecules present in the soaked crystal or cocrystal structures, respectively.

Source (NSLS) at Brookhaven National Laboratory and were processed using *HKL*-2000 (Otwinowski & Minor, 1997). Data were collected from the cocrystal using our in-house facility (RU-H3R generator, Osmic optics, R-AXIS IV^{++} detector) and processed using *d*TREK* (Pflugrath, 1999). The data-collection and refinement statistics are presented in Table 1.

2.3. Structure solution

The crystals of the inhibitor complexes are isomorphous to the native protein crystals (Lobsanov *et al.*, 2002), which allowed us to determine the structures by using difference Fourier methods. For each set of data (cocrystal and soak in Table 1), the protein atoms of the fungal α-1,2-mannosidase (PDB code 1kkt) were subjected to rigid-body refinement in *CNS* (Brünger *et al.*, 1998). No water molecules or calcium ions from the model were included and each monomer was treated as a rigid body. 7% of the structure factors were randomly selected for cross-validation (Brünger, 1992) and were excluded from all steps of the refinement. The resulting σ_A-weighted difference and $2F_o - F_c$ maps revealed strong density corresponding to the calcium ions and ordered solvent molecules (Fig. 2). In the soaked crystals, strong density was observed for the intact LM disaccharide (Fig. 2*b*). No inhibitor

density was found in the cocrystals (Fig. 2a). Refinement of the models using the simulated-annealing slow-cooling protocol (Brünger *et al.*, 1990) was monitored by R_{free} and
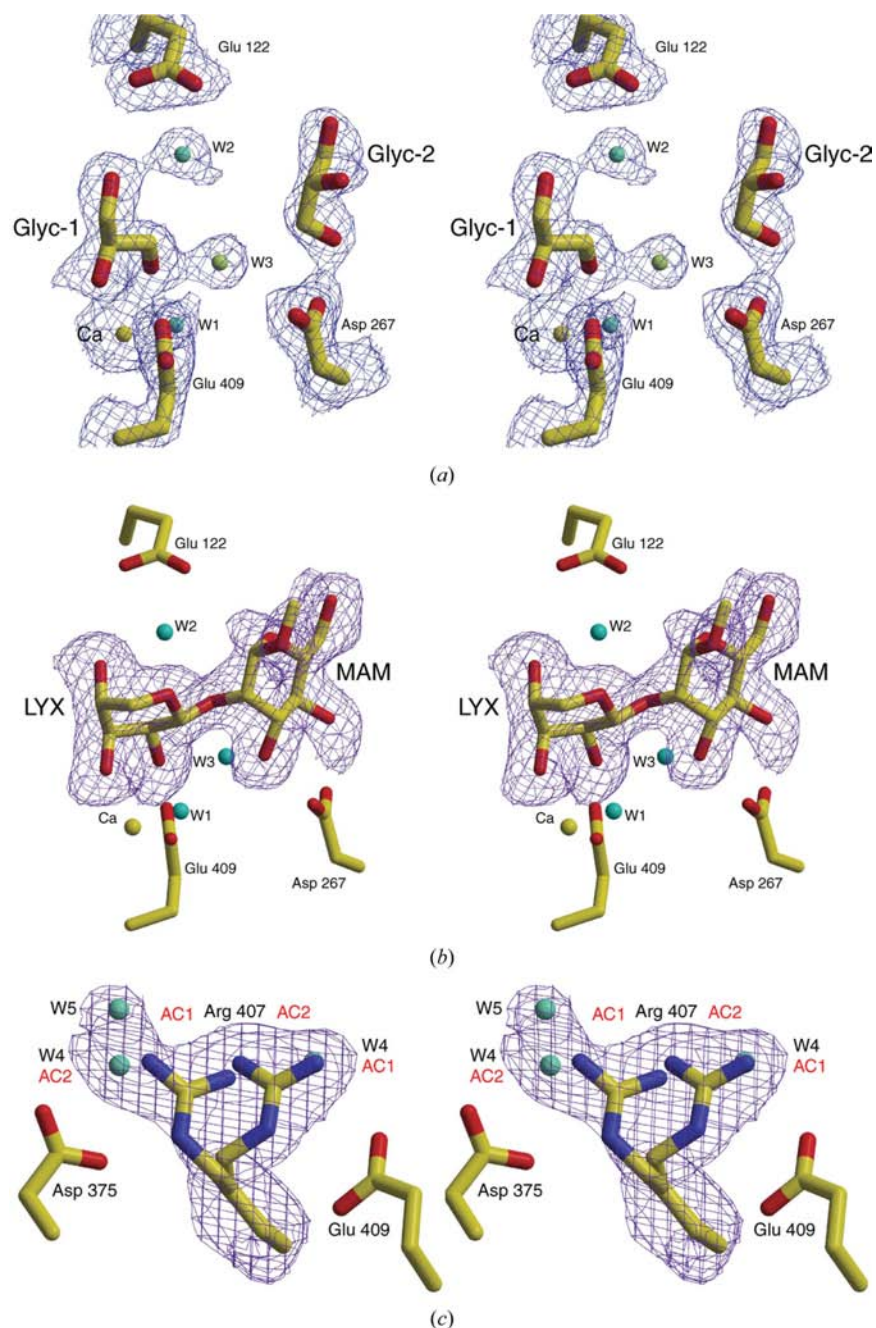

(a)

(b)

(c)

Figure 2
Stereoviews showing the electron density found in the active-site region for (a) the cocrystal and (b, c) the soaked data. In (a), only solvent molecules, waters W1 and W2 and glycerol (Glyc-1 and Glyc-2) are present in the active site. In (b), electron density for the D-lyxoside (LYX) and methyl-α-mannoside (MAM) moieties of the intact LM disaccharide is clearly visible. In (a) and (b) the side chains of the residues previously implicated in the catalytic mechanism, Glu122, Asp267 and Glu409, are shown as ball-and-stick models. The essential calcium ion (Ca) and water molecules are shown as yellow and cyan spheres, respectively. In (c) the side chains of residues Asp375, Arg407 and Glu409 are shown as ball-and-stick models. Both the AC1 and AC2 alternative conformations of Arg407 are shown with the water molecule W4 in its AC1 and AC2 alternative positions. The AC1 and AC2 conformations or positions are 25% and 75% occupied, respectively. An extra water molecule W5 has a single full-occupancy position. In (a) the final σ_{A}-weighted $2F_{\text{o}} - F_{\text{c}}$ and in (b) and (c) $F_{\text{o}} - F_{\text{c}}$ electron-density OMIT maps are contoured at 1σ and 2σ, respectively.

alternated with manual inspection and rebuilding using *Xfit* (McRee, 1999). No NCS restraints were used in the refinements; the two monomers in the asymmetric unit were rebuilt and refined independently of each other. During the course of the refinement our difference Fourier maps revealed nonuniform negative density in the active site. Alternative conformations were modelled for the LM, the glycerol molecules and Arg407. The percentage occupancy of each alternative conformation was varied until the best correlation between positive and negative difference density was achieved. The temperature factors of atoms that interact were also monitored and used to confirm the validity of the occupancies used. The final models for each monomer in the two structures contain 475 amino-acid residues (residues 36–510), one calcium ion and nine carbohydrate residues in three N-linked oligosaccharide chains. One LM molecule (75% occupancy) and two glycerol molecules (25% occupancy) in each monomer as well as 717 water molecules were included in the soaked crystal structure, while four glycerol molecules (monomer *A*) and three glycerol molecules (monomer *B*) and 692 water molecules were included in the cocrystal structure. The model for the D-lyxoside moiety was generated using mannose and replacing the CH$_2$OH group at the C5 position with a H atom. The resulting D-lyxoside model was rebuilt in *Xfit* to generate all possible ring conformations. The $^1C_4$ conformation of D-lyxoside was the most consistent with the experimental density (Fig. 2b). The *CNS* topology and parameter information for the D-lyxoside moiety were created by modifying the corresponding mannose data files. In order to better reflect the effectively equatorial position of the glycosidic bond of α-lyxose in the $^1C_4$ ring conformation, the B12 patch for the α-1,2 linkage between D-lyxose and mannose was used in *CNS* refinement. No other geometric constraints for the ligand were used in the refinement in order to allow the inhibitor model to fully reflect the experimental data. There are no protein residues in disallowed regions of the Ramachandran plot as determined using *PROCHECK* (Laskowski *et al.*, 1993). Approximately 85% of the residues in the two structures lie in the most favoured regions. The values of R and R_{free}, as well as the percentage of residues in the most favoured region of the Ramachandran plot,

reflect disordered loop regions (particularly in the second monomer, monomer B) where the density is present but uninterpretable.

2.4. Structural comparisons

Superimpositions were performed with *LSQMAN* (Kleywegt, 1999) using either all C^{α} atoms of the protein or the extended main-chain atoms (C^{α}, N, C, O and C^{β}) of the ten conserved active-site residues Phe121, Glu122, Arg126, Asp267, Leu330, Arg407, Glu409, Phe468, Glu472 and Glu502.

2.5. Mass-spectrometric analysis

ESI–Q-TOF mass-spectrometric data were collected on a 5 mM solution of LM in deionized water and from a fungal α-1,2-mannosidase–LM solution (5 mM LM, 9 mg ml^{-1} or 0.2 mM protein, 1.5 mM sodium acetate pH 5.0, the pH of optimum activity for this enzyme) after 0 and 24 h incubation.

3. Results and discussion

3.1. Methyl-α-D-lyxopyranosyl-(1′,2)-α-D-mannopyranoside is a hydrolyzable substrate analogue

Cocrystals of the fungal α-1,2-mannosidase with LM (Fig. 1b) were grown over several days and were flash-frozen prior to data collection using glycerol as a cryoprotectant. The electron density in the −1/+1 subsites of the active site of these crystals is consistent with the presence of only glycerol and water molecules (Fig. 2a). Data collected at room temperature on a cocrystal which had not been exposed to glycerol only showed electron density in the −1/+1 subsites consistent with water molecules (data not shown). Both the low-temperature and room-temperature cocrystal data indicate that LM is not bound to the protein. This was unexpected as LM had previously been shown to be a competitive inhibitor (K_{i} = 0.6 mM) of the closely homologous α-1,2-mannosidase from *Hypocrea jecorina* (Desmet *et al.*, 2002). Given the concentrations of LM and fungal α-1,2-mannosidase used (5 mM and ∼0.2 mM, respectively), we expected the inhibitor to be bound to the protein in the cocrystallization experiment.

Mass-spectrometry data on a fungal α-1,2-mannosidase–LM solution, where the reagents were mixed at the same concentrations used in the cocrystallization experiment, indicated that the entire LM compound had been hydrolysed after 24 h (data not shown). Taken together, the cocrystallization and mass-spectrometry data suggest that when LM is incubated with the mannosidase for long periods of time it is cleaved and that LM behaves as a substrate.

3.2. Fungal α-1,2-mannosidase–LM complex and alternative conformations observed for Arg407

In an attempt to obtain the structure of the intact LM prior to hydrolysis, we soaked native fungal α-1,2-mannosidase crystals in a concentrated LM solution for short periods of time prior to data collection. The data obtained from a crystal soaked for 10 min in a series of solutions containing increasing concentrations of LM to a final concentration of 9 mM (see §2) revealed electron density for the intact methyl-α-D-lyxopyranosyl-(1′,2)-α-D-mannopyranoside spanning the −1/+1 subsites. The occupancy of the LM was refined to 75%. The D-lyxoside moiety is found in the −1 subsite, while the methyl-D-mannoside moiety occupies the +1 subsite (Fig. 2b). The interactions between LM and the protein are detailed in Fig. 3. Density corresponding to two glycerol
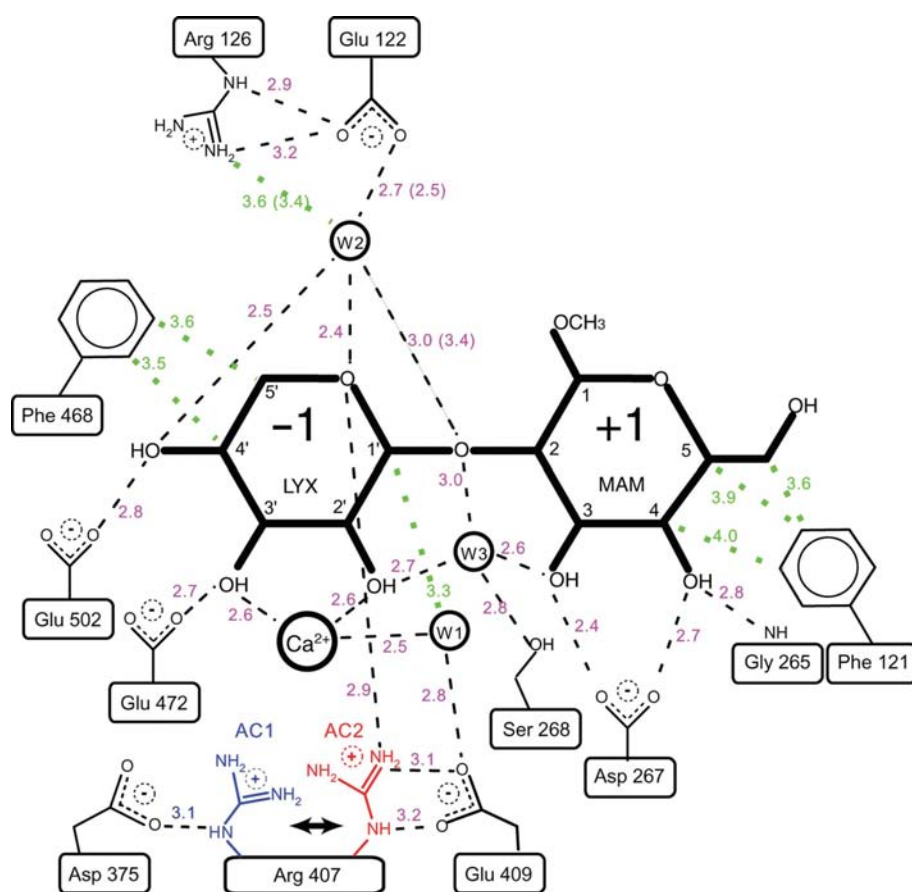

Figure 3
Schematic representation of the interactions between the D-lyxoside (LYX) and methyl-α-mannoside (MAM) moieties of LM in the −1 and +1 subsites and the fungal α-1,2-mannosidase protein. Hydrogen bonds ($\leq$3.2 Å) are shown by dashed lines. Nonpolar van der Waals interactions are shown as green dotted lines. The three water molecules and the calcium ion found to interact with the disaccharide are represented as circles and labelled W1, W2, W3 and Ca^{2+}, respectively. Distances in angstroms are given for monomer A. The corresponding distances in monomer B that deviate by greater than 0.2 Å are reported in parentheses.

molecules (25% occupancy) was also evident and was modelled. The glycerol molecules are found in the same location as seen in the cocrystal structure (Fig. 2a).

The D-lyxoside moiety in the −1 subsite adopts the $^1C_4$ inverted-chair conformation (Fig. 2b) in the same position and conformation as observed previously for dMNJ and KIF in the fungal α-1,2-mannosidase structures complexed with these inhibitors (Lobsanov et al., 2002; Fig. 4a). For clarity only dMNJ has been shown in Fig. 4; please refer to Lobsanov et al. (2002) for details of the superposition of dMNJ and KIF. The O2′ and O3′ hydroxyl groups of the D-lyxoside moiety (LYX) are in direct contact with the Ca^{2+} ion, while the C1′ anomeric carbon is at a van der Waals distance from water molecule W1 (Fig. 2b and 3). This $^1C_4$ conformation appears to be favoured by interactions with the calcium ion and Phe468 (Fig. 3), as noted previously (Vallée, Karaveg et al., 2000). The presence of an aromatic residue in the catalytic site of many glycoside hydrolases and its importance for proper positioning of a carbohydrate substrate have been reported previously (Nerinckx et al., 2003). The absence of the C5′ hydroxymethyl moiety and the missing interaction of its O6 hydroxyl with the protein do not prevent the LM in the fungal α-1,2-mannosidase–LM complex from binding in the same position and conformation as the dMNJ and KIF inhibitors (Lobsanov et al., 2002; Fig. 4a).

The methyl-α-D-mannoside moiety (MAM) in the +1 subsite is found in the ground-state $^4C_1$ chair conformation in approximately the same position and orientation as the M7 (0.36–0.51 Å between corresponding ring atoms; Fig. 4b) and M6 (0.63–1.15 Å) D-mannose residues (Fig. 1a) observed in the yeast ER mannosidase (Vallée, Lipari et al., 2000) and mouse Golgi mannosidase IA (Tempel et al., 2004) structures, respectively. In each of these structures, a high-mannose oligosaccharide from one molecule extends into the barrel of an adjacent symmetry-related molecule in what is apparently an enzyme–product complex. The O2 glycosidic O atom of MAM is found to interact with two water molecules, W2 and W3, which in turn are hydrogen bonded to Glu122 and Ser268, respectively (Figs. 2b and 3).

Examination of the active site of the fungal α-1,2-mannosidase–LM complex reveals that Arg407 in both monomers A and B is present in two alternative conformations, AC1 and AC2, at 25% and 75%

occupancy, respectively (Figs. 2c, 3 and 4a). One of these conformations (AC2; Fig. 2c) is unique to the fungal α-1,2-mannosidase–LM complex and has not been observed in any previously determined mannosidase structure. In the AC2 conformation, Arg407 $N^{η2}$ is in contact with the O5′ ring O atom of the D-lyxoside moiety of LM (Figs. 3 and 4a). In this conformation, Arg407 $N^{ε}$ and Arg407 $N^{η2}$ also interact with Glu409 $O^{ε1}$ and Glu409 $O^{ε2}$. In the previously determined
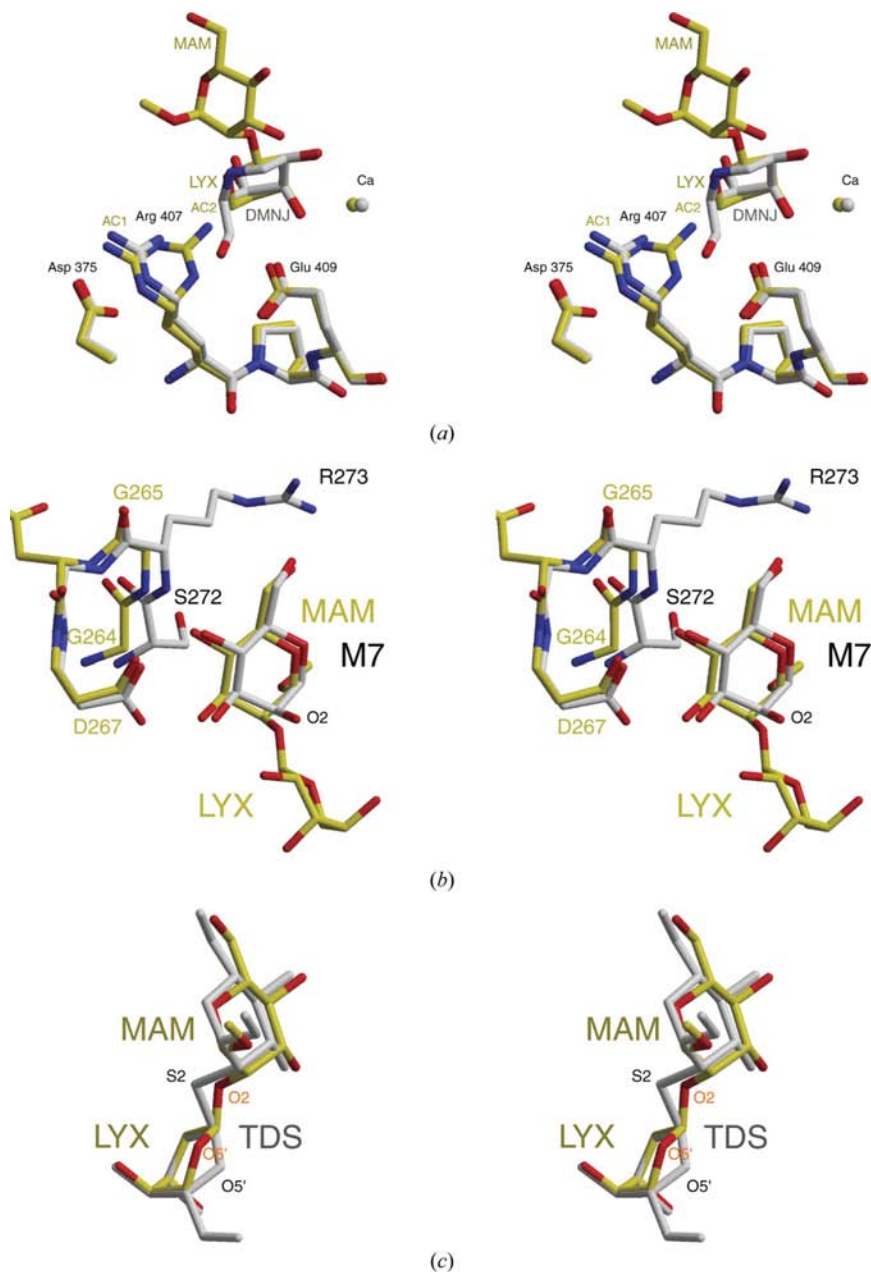

Figure 4
Stereo-superimposition of LM with (a) dMNJ, (b) the M7 moiety of N-glycan and (c) a thiodisaccharide inhibitor. In each case the D-lyxoside (LYX) and methyl-α-mannoside (MAM) moieties are shown as ball-and-stick models with C and O atoms in yellow and red, respectively. In (a) the dMNJ, shown in grey, is from the fungal α-1,2-mannosidase–dMNJ structure (PDB code 1kre; Lobsanov et al., 2002), in (b) the M7 mannose, shown in grey, is from the yeast α-1,2-mannosidase structure (PDB code 1dl2; Vallée, Lipari et al., 2000) and in (c) the thiodisaccharide inhibitor (TDS), shown in grey, is from the human α-1,2-mannosidase–TDS structure (PDB code 1x9d; Karaveg et al., 2005).

structures of native fungal α-1,2-mannosidase and its complexes with dMNJ and KIF, Arg407 is found in a single conformation with its N^{ε} atom interacting with either Asp375 $O^{\delta 1}$ or, in the complex structures, with both Asp375 and the O6 hydroxyl group of dMNJ or KIF (Lobsanov et al., 2002). The implications of the interaction between Arg407 and Glu409 are discussed below.

3.3. Comparison with the human α-1,2-mannosidase–thiodisaccharide complex

A comparison of the fungal α-1,2-mannosidase–LM structure with the structure of the human ER mannosidase in complex with a thiodisaccharide (TDS) spanning the $-1/+1$ subsites (Karaveg et al., 2005) reveals that the LM is in a very similar position to that observed for the TDS. However, in the human α-1,2-mannosidase–TDS complex, the glycon in the -1 subsite is in the $^3S_1$ conformation with an axial anomeric substituent, whereas the D-lyxoside in the fungal α-1,2-mannosidase–LM complex shows the $^1C_4$ conformation with an equatorial anomeric positioning (Fig. 4c). The C5′ hydroxymethyl group of the nonreducing end D-mannoside of TDS is positioned similarly to those at C5 of dMNJ and KIF in the corresponding human and fungal α-1,2-mannosidase complex structures (Vallée, Karaveg et al., 2000; Lobsanov et al., 2002). The D-mannoside glycon of TDS superimposes well with the D-lyxoside moiety of LM, whereas the methyl-D-mannoside occupying the $+1$ subsite is shifted in comparison to that of LM. This shift has both lateral (in-the-ring) and orthogonal (off-the-ring) components. This is likely to be the result of the axial versus equatorial anomeric glycon configuration, as well as the longer thioglycosidic bond in TDS

compared with the O-glycosidic bond in LM. With a smaller bridge angle of $106.1°$ compared with $117.3°$ in LM and the 0.4 Å longer C1′—S and S—C2 bonds in the thiol linkage of TDS, its sulfur position is displaced 0.8 Å from the position of the O atom in the O-glycosidic linkage in the superposed LM (Fig. 4c). The major positional difference between the glycon-ring atoms of LM and TDS is at their respective O5′ ring O atoms (Fig. 4c). In terms of torsion angles, this displacement of 1.0 Å translates into two rotations around the C4′—C5′ and C2′—C1′ bonds of $42.6°$ and $46.1°$, respectively.

3.4. Catalytic residues and reaction itinerary

Class I α-1,2-mannosidases are inverting glycoside hydrolases that specifically cleave the α-1,2-glycosidic linkage with inversion of anomeric configuration. The catalytic mechanism for this class of inverting enzymes is atypical (Vallée, Karaveg et al., 2000) as two water molecules are directly involved rather than one. Based on previous structures of the human ER mannosidase with the aza-mannose mimics dMNJ and KIF, either Glu409 or Asp267 were suggested to play the role of the water-nucleophile activating catalytic base (Vallée, Karaveg et al., 2000). Our fungal α-1,2-mannosidase–LM stucture as well as that of the human α-1,2-mannosidase–TDS (Karaveg et al., 2005) complex suggest that Glu409 is the catalytic base. Indeed, in the fungal α-1,2-mannosidase–LM complex the water molecule that is the closest to the anomeric carbon C1′ on the β-face is W1 (Fig. 3), one of four water molecules coordinating the Ca^{2+} ion. This water in turn interacts with Glu409 $O^{\varepsilon 1}$ (2.8 and 2.6 Å in monomers A and B, respectively). The side-chain carboxylate of Asp267 on the other hand is over 4 Å away from W1 (4.8 Å in both monomers A
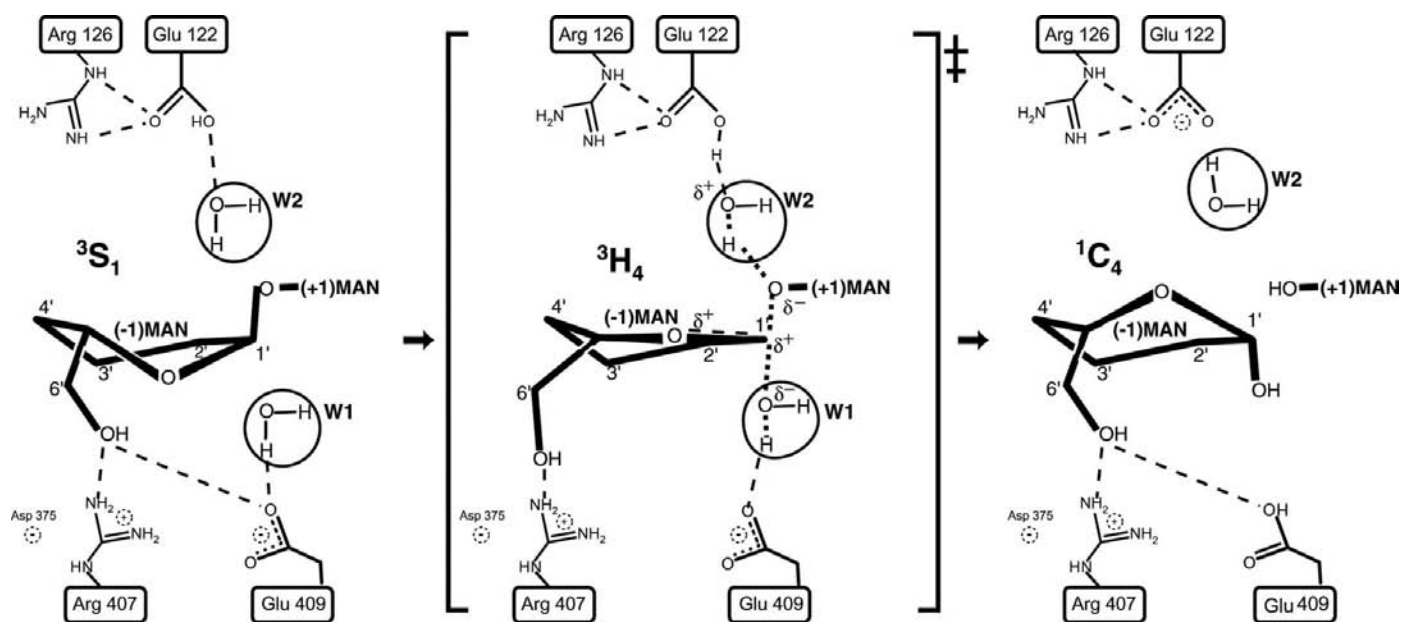

Figure 5
Proposed mechanism for P. citrinum α-1,2-mannosidase-catalyzed hydrolysis. For simplicity, the O2′, O3′ and O4′ hydroxyls that are fixed to the protein groups and the calcium ion are not shown. The substrate binds in the -1 subsite in the α-$^3S_1$ conformation. A $^3H_4$ transition-state conformation is implicated prior to formation of the β-$^1C_4$ inverted product, with subsequent release of the product in the $^4C_1$ conformation.

and *B*) and instead appears to play a role in substrate recognition towards the C3 and C4 hydroxyl groups of the D-mannoside unit in the +1 subsite (Fig. 3).

Glu122 has been proposed to play the role of an indirect acid catalyst (Vallée, Karaveg *et al.*, 2000) by transferring a proton to a water molecule (W2) which is in contact with the glycosidic O atom of the substrate. The protonation machinery may even be more complex, since this Glu122 residue is within ion-pairing distance of Arg126, which is embedded in an extensive network of polar interactions, and instead a Glu122–Arg126–W2 triad complex (fungal α-1,2-mannosidase numbering) may play the role of the general acid in the catalytic mechanism as previously suggested by the authors of the human α-1,2-mannosidase–TDS structure (Karaveg *et al.*, 2005). Kinetic studies on mutants of different members of the class I mannosidase family (Lipari & Herscovics, 1999; Karaveg & Moremen, 2005; Tatara *et al.*, 2003) are consistent with the role of Glu409 as the catalytic base and the Glu122–Arg126–W2 triad as a proton-donor system. The distance between Glu409 $O^{\varepsilon 1}$ (catalytic base) and water W2 is 7.0 Å, which is within the limits of the empirically derived range of 6.5–9.5 Å between catalysts in an inverting glycosidase mechanism (Davies & Henrissat, 1995). In the fungal α-1,2-mannosidase–LM structure there is a second water molecule, W3, near the O2 leaving group of MAM (3.10 and 2.8 Å in monomers *A* and *B*, respectively; Figs. 2*b* and 3) and this water bridges to the O^{γ} atom of the conserved Ser268 (2.8 and 3.3 Å in monomers *A* and *B*, respectively). While W3 is at the same distance as W2 from the O2 leaving group and is a potential member of another proton-donor system, it is unlikely that Ser268 protonates W3, unless Asp267 $O^{\delta 2}$, which is $\sim$3.5 Å away, can facilitate the loss of a proton.

The α-axial $^3S_1$ glycon conformer observed in the human α-1,2-mannosidase–TDS complex is a revealing indication of the conformational itinerary of the enzyme-catalyzed hydrolysis reaction (Karaveg *et al.*, 2005). Such a glycon conformer complies with the Antiperiplanar Lone Pair Hypothesis (ALPH; Deslongchamps, 1993) and is indicative of passage through the conformationally nearby $^3H_4$-like transition state (Fig. 5). This is corroborated by a recent docking study on the yeast α-1,2-mannosidase enzyme (Mulakala *et al.*, 2006, 2007) as well as a recent theoretical study (Nerinckx *et al.*, 2006; Mulakala *et al.*, 2006). The observed α-$^1C_4$ D-lyxoside in the fungal α-1,2-mannosidase–LM complex is unlikely to be a productive conformer since the scissile bond is equatorial and as such non-ALPH-compliant. It is instead a local minimum that is reminiscent of the end of the reaction itinerary, *i.e.* the β-$^1C_4$ inverted-chair conformer (Fig. 5). Indeed, the -1 subsite of glycoside hydrolase family GH47 enzymes appears to have a preference for the $^1C_4$ inverted chair, since this is observed with the dMNJ inhibitor as well as in our fungal α-1,2-mannosidase–LM complex, although dMNJ (Vallée, Karaveg *et al.*, 2000) and D-lyxose (Stoddard, 1971) both have a $^4C_1$ ground-state conformation.

The $^3H_4$ half-chair conformation is achieved when the O5′ atom is midway between the two positions in the observed $^1C_4$ and $^3S_1$ conformations (0.5 Å). This is equivalent to rotations

around the C4′—C5′ and C2′—C1′ bonds of 21.3° and 23.1°, respectively. Supporting a $^3H_4$ transition state and consistent with the principle of the least atomic motion (Hine, 1977) is the fact that movement of the O5′ atom along the reaction path would not alter the positions of the O2′, O3′ and O4′ atoms, which are anchored in the structure by the calcium ion, Glu472 and Glu502 (Fig. 3).

3.5. Role of the C5′ hydroxymethyl group and Arg407 and Asp375 in catalysis

The importance of the C5′ hydroxymethyl group in catalysis has been noted previously for another glycosidase (Zou *et al.*, 1999) and was the rationale for the design of the methyl-α-D-lyxopyranosyl-(1′,2)-α-D-mannopyranoside as a potential inhibitor (Desmet *et al.*, 2002). The only difference between LM and the minimal natural substrate, mannobiose, is the lack of a hydroxymethyl moiety on the C5′ atom (Fig. 1*b*). The lack of this group leads to two alternative conformations for Arg407 (Figs. 3 and 4*a*). The presence of the second AC2 conformation for Arg407 observed in the fungal α-1,2-mannosidase–LM structure (Fig. 2*c*) is likely to be the result of the void created by the lack of the C5′ hydroxymethyl group, which can be occupied by the arginine side chain. It is interesting to note that in this conformation Arg407 interacts with Glu409, likely neutralizing this residue and perturbing its role as the catalytic base. This suggests that the role of the C5′ arm in catalysis is to prevent Arg407 from interacting with Glu409 and hence deactivating the catalytic base. The observed ratio of the active AC1 to the inactive AC2 conformation of Arg407 observed in the crystal structure is 25% to 75% or 1:3. This is the same ratio as found for the occupancies of the two glycerol molecules (25% occupancy) and the uncleaved lyxomannoside (75% occupancy) in the active site. The presence of the active AC1 conformation and glycerol molecules is consistent with the observed slow hydrolysis of LM by the enzyme in the crystals (see §3.1). These data support the suggested role of Arg407 as a modulator of enzyme activity. In all inhibitor-complex structures determined to date in which a C5′ moiety is present, Arg407 is seen to interact with the O6 hydroxyl of this moiety. The C5′ arm would sterically prevent Arg407 from occurring in the AC2 conformation. In the AC1 conformation Arg407 interacts with Asp375 (Figs. 2*c*, 3 and 4*a*).

Our structure suggests that enzyme activity is compromised when Arg407 is in the AC2 conformation, forming a salt bridge with Glu409, but that the enzyme is active when Arg407 is in the AC1 conformation, forming a salt bridge with Asp375 (Figs. 3 and 4*a*). The importance of Asp375 in catalysis has been demonstrated previously by the chemical treatment of the fungal α-1,2-mannosidase with 1-ethyl-3-(3-dimethylaminopropyl)carbodiimide (Yoshida *et al.*, 1994). This compound was shown to almost completely inactivate the fungal enzyme by modifying Asp375 to an imide group, with partial protection against inactivation occurring in the presence of dMNJ. Our fungal α-1,2-mannosidase–LM structure provides an explanation for this inactivation, as chemical modification of Asp375 that eliminated the negative charge on

this residue would disrupt the electrostatic interaction between Asp375 and Arg407, forcing Arg407 to assume the AC2 conformation and hence inactivating the enzyme. The observation that dMNJ only partially protects against inactivation is consistent with the proposed model of interactions as Asp375 is still solvent-accessible after dMNJ binding. Rather, the bound dMNJ would lock Arg407 into the active AC1 conformation where it would interact with Asp375 and hence be less accessible for modification by the carbodiimide. Taken together, the structural and chemical data suggest that the presence or absence of a negative charge on Asp375 thus corresponds to the active or inactive conformations of Arg407, respectively. The role of Asp375 in catalysis would therefore appear to be the maintenance of the active AC1 conformation of Arg407, while Arg407 appears to modulate activity. Interestingly, Arg407 is strictly conserved across the superfamily. Sequence comparisons of the 278 members of superfamily GH47 allow us to define a conserved sequence motif RPExxE, which includes Arg407, the catalytic base Glu409 and Glu412, which is involved in coordinating the essential calcium ion. This motif appears to be important for modulating enzyme activity. Mutation of the equivalent arginine in human α-1,2-mannosidase reveals that this residue is critical not only for activity but potentially for the stability of the protein, as expression of the R334A mutant could not be detected (Karaveg *et al.*, 2005). Sequence comparisons also show that the carboxylate group of Asp375 is also highly conserved as either an Asp or Glu.

3.6. N-Glycan interactions and modification of Arg407 conformation

Asp375 and Arg407 are also involved in interactions with the N-glycan in the +2/+3 subsites. In the yeast ER mannosidase structure (Vallée, Lipari *et al.*, 2000) the mannose in the +2 subsite (M4 in Fig. 1*a*) forms a direct hydrogen bond to the guanidinium group of Arg433 (equivalent to Arg407 in the fungal α-1,2-mannosidase structure), while the carboxylate group of Glu399 (equivalent to Asp375 in the fungal α-1,2-mannosidase) is in direct contact with the O6 of the mannose in the +3 subsite (M6 in Fig. 1*a*). It would appear, at least in the yeast ER enzyme, that the interaction between the N-glycan and the protein favours the active AC1 conformation of the arginine (Arg407 in fungal α-1,2-mannosidase). Interestingly, although we found no LM in the active site of our cocrystal structure, several glycerol molecules were present (*e.g.* Fig. 2*a*) and these also appear to influence the conformation of Arg407. Glycerol is well known for its propensity to bind to proteins in carbohydrate-binding sites (Vallée, Lipari *et al.*, 2000). In our cocrystal structure, a glycerol is found in the +2 subsite in direct contact with Arg407. This interaction is slightly different in monomers *A* and *B* and results in two different conformations for Arg407. In one monomer Arg407 adopts the inactive AC2 conformation, while in the second monomer its conformation is intermediate between the active AC1 and inactive AC2 conformations. Intermediate conformations of the Arg407 equivalents are also observed in the

ligand-free human α-1,2-mannosidase and *Trichoderma reesei* α-1,2-mannosidase structures cryoprotected using glycerol and PEG 200, respectively (Vallée, Karaveg *et al.*, 2000; Van Petegem *et al.*, 2001). The data thus suggest that Arg407 is flexible and can accept a range of conformations depending on the interactions in the +2 subsite of the N-glycan.

4. Conclusion

Our structure of intact LM spanning the −1/+1 subsites of a mannosidase with the D-lyxoside ring observed in the $^1C_4$ conformation has allowed us to further investigate the catalytic residues and to describe the details of the catalytic mechanism (Fig. 5). The water molecule W1, activated by the catalytic base Glu409, performs the nucleophilic attack on the C1′ catalytic centre on its β-face in an S_N2-like reaction, thereby inverting the anomeric configuration at the C1′ of the reaction product. The leaving group, the O2 of the +1 subsite residue, appears likely to be protonated by a second water molecule W2 assisted by the Glu122/Arg126 dyad. The transition-state conformation of the natural substrate is suggested to be at or near $^3H_4$. An alternative conformation of the side chain of Arg407, in direct contact with D-lyxoside and Glu409, is found in the fungal α-1,2-mannosidase–LM structure and its presence is a consequence of the absence of the C5′ hydroxymethyl group in the D-lyxoside moiety. The formation of a salt bridge between Arg407 and Glu409 could neutralize a negative charge on Glu409, thus deactivating it as the catalytic base. The role of the C5′ arm in catalysis appears to prevent such an event. The alternative conformations of Arg407 have also highlighted the importance of the network of interactions between Asp375, Arg407 and N-glycan in the +2/+3 glycan subsites in catalysis and suggest that Arg407, which belongs to the conserved sequence motif RPExxE, appears to regulate the activity of the enzyme.

References

Brünger, A. T. (1992). *Nature (London)*, **355**, 472–474.
Brünger, A. T., Adams, P. D., Clore, G. M., DeLano, W. L., Gros, P., Grosse-Kunstleve, R. W., Jiang, J.-S., Kuszewski, J., Nilges, M., Pannu, N. S., Read, R. J., Rice, L. M., Simonson, T. & Warren, G. L. (1998). *Acta Cryst.* D**54**, 905–921.

research papers

Brünger, A. T., Krukowski, A. & Erickson, J. W. (1990). *Acta Cryst.* A**46**, 585–593.

Camirand, A., Heysen, A., Grondin, B. & Herscovics, A. (1991). *J. Biol. Chem.* **266**, 15120–15127.

Davies, G. & Henrissat, B. (1995). *Structure*, **3**, 853–859.

Deslongchamps, P. (1993). *Pure Appl. Chem.* **65**, 1161–1178.

Desmet, T., Nerinckx, W., Stals, I., Callewaert, N., Contreras, R. & Claeyssens, M. (2002). *Anal. Biochem.* **307**, 361–367.

Gonzalez, D. S., Karaveg, K., Vandersall-Nairn, A. S., Lal, A. & Moremen, K. W. (1999). *J. Biol. Chem.* **274**, 21375–21386.

Haltiwanger, R. S. & Lowe, J. B. (2004). *Annu. Rev. Biochem.* **73**, 491–537.

Helenius, A. & Aebi, M. (2004). *Annu. Rev. Biochem.* **73**, 1019–1049.

Henrissat, B. & Bairoch, A. (1996). *Biochem J.* **316**, 695–696.

Herscovics, A. (1999). *Biochim. Biophys. Acta*, **1473**, 96–107.

Herscovics, A. (2001). *Biochimie*, **83**, 757–762.

Hine, J. (1977). *Adv. Phys. Org. Chem.* **15**, 1–61.

Hirao, K., Natsuka, Y., Tamura, T., Wada, I., Morito, D., Natsuka, S., Romero, P., Sleno, B., Tremblay, L. O., Herscovics, A., Nagata, K. & Hosokawa, N. (2006). *J. Biol. Chem.* **281**, 9650–9658.

Hosokawa, N., Wada, I., Hasegawa, K., Yorihuzi, T., Tremblay, L. O., Herscovics, A. & Nagata, K. (2001). *EMBO Rep.* **2**, 415–422.

Jakob, C. A., Bodmer, D., Spirig, U., Battig, P., Marcil, A., Dignard, D., Bergeron, J. J., Thomas, D. Y. & Aebi, M. (2001). *EMBO Rep.* **2**, 423–430.

Karaveg, K. & Moremen, K. W. (2005). *J. Biol. Chem.* **280**, 29837–29848.

Karaveg, K., Siriwardena, A., Tempel, W., Liu, Z.-J., Glushka, J., Wang, B.-C. & Moremen, K. W. (2005). *J. Biol. Chem.* **280**, 16197–16207.

Kleywegt, G. J. (1999). *Acta Cryst.* D**55**, 1878–1884.

Lal, A., Pang, P., Kalelkar, S., Romero, P. A., Herscovics, A. & Moremen, K. W. (1998). *Glycobiology*, **8**, 981–995.

Laskowski, R. A., MacArthur, M. W., Moss, D. S. & Thornton, J. M. (1993). *J. Appl. Cryst.* **26**, 283–291.

Lipari, F. & Herscovics, A. (1999). *Biochemistry*, **38**, 1111–1118.

Lobsanov, Y. D., Vallée, F., Imberty, A., Yoshida, T., Yip, P., Herscovics, A. & Howell, P. L. (2002). *J. Biol. Chem.* **277**, 5620–5630.

Lowe, J. B. & Marth, J. D. (2003). *Annu. Rev. Biochem.* **72**, 643–691.

McRee, D. E. (1999). *J. Struct. Biol.* **125**, 156–165.

Mast, S. W., Diekman, K., Karaveg, K., Davis, A., Sifers, R. N. & Moremen, K. W. (2005). *Glycobiology*, **15**, 421–436.

Mulakala, C., Nerinckx, W. & Reilly, P. J. (2006). *Carbohydr. Res.* **341**, 2233–2245.

Mulakala, C., Nerinckx, W. & Reilly, P. J. (2007). *Carbohydr. Res.* **342**, 163–169.

Nakatsukasa, K., Nishikawa, S., Hosokawa, N., Nagata, K. & Endo, T. (2001). *J. Biol. Chem.* **276**, 8635–8638.

Nerinckx, W., Desmet, T. & Claeyssens, M. (2003). *FEBS Lett.* **538**, 1–7.

Nerinckx, W., Desmet, T. & Claeyssens, M. (2006). *Arkivoc*, **13**, 90–116.

Olivari, S., Cali, T., Salo, K. E., Paganetti, P., Ruddock, L. W. & Molinari, M. (2006). *Biochem. Biophys. Res. Commun.* **349**, 1278–1284.

Olivari, S., Galli, C., Alanen, H., Ruddock, L. & Molinari, M. (2005). *J. Biol. Chem.* **280**, 2424–2428.

Olivari, S. & Molinari, M. (2007). *FEBS Lett.* **581**, 3658–3664.

Otwinowski, Z. & Minor, W. (1997). *Methods Enzymol.* **276**, 307–326.

Pflugrath, J. W. (1999). *Acta Cryst.* D**55**, 1718–1725.

Spiro, R. G. (2004). *Cell. Mol. Life Sci.* **61**, 1025–1041.

Stoddard, J. F. (1971). *Stereochemistry of Carbohydrates.* New York: Wiley-Interscience.

Tatara, Y., Lee, B. R., Yoshida, T., Takahashi, K. & Ichishima, E. (2003). *J. Biol. Chem.* **278**, 25289–25294.

Tempel, W., Karaveg, K., Liu, Z.-J., Rose, J., Wang, B.-C. & Moremen, K. W. (2004). *J. Biol. Chem.* **279**, 29774–29786.

Tremblay, L. O. & Herscovics, A. (1999). *Glycobiology*, **9**, 1073–1078.

Tremblay, L. O. & Herscovics, A. (2000). *J. Biol. Chem.* **275**, 31655–31660.

Trombetta, E. S. & Parodi, A. J. (2003). *Annu. Rev. Cell Dev. Biol.* **19**, 649–676.

Vallée, F., Karaveg, K., Herscovics, A., Moremen, K. W. & Howell, P. L. (2000). *J. Biol. Chem.* **275**, 41287–41298.

Vallée, F., Lipari, F., Yip, P., Sleno, B., Herscovics, A. & Howell, P. L. (2000). *EMBO J.* **19**, 581–588.

Van Petegem, F., Contreras, H., Contreras, R. & Van Beeumen, J. (2001). *J. Mol. Biol.* **312**, 157–165.

Varki, A. (1993). *Glycobiology*, **3**, 97–130.

Yoshida, T. & Ichishima, E. (1995). *Biochim. Biophys. Acta*, **1263**, 159–162.

Yoshida, T., Maeda, K., Kobayashi, M. & Ichishima, E. (1994). *Biochem. J.* **303**, 97–103.

Yoshida, T., Nakajima, T. & Ichishima, E. (1998). *Biosci. Biotechnol. Biochem.* **62**, 309–315.

Zou, J., Kleywegt, G. J., Stahlberg, J., Driguez, H., Nerinckx, W., Claeyssens, M., Koivula, A., Teeri, T. T. & Jones, T. A. (1999). *Structure Fold. Des.* **7**, 1035–1045.